FITEE

Fused-like angles: replacement for roll-pitch-yaw angles for a six-degree-of-freedom grating interferometer[*]

Di CHANG[1,2], Pengcheng HU[‡1,2], Jiubin TAN[1,2]

[1]*Center of Ultra-precision Optoelectronic Instrument Engineering, Harbin Institute of Technology, Harbin 150080, China*

[2]*Key Lab of Ultra-precision Intelligent Instrumentation (Harbin Institute of Technology),*

Ministry of Industry and Information Technology, Harbin 150080, China

E-mail: di.chang@hit.edu.cn; hupc@hit.edu.cn; jbtan@hit.edu.cn

Abstract: Representation of orientation is important in a six-degree-of-freedom grating interferometer but only a few studies have focused on this topic. Roll-pitch-yaw angles, widely used in aviation, navigation, and robotics, are now being brought to the field of multi-degree-of-freedom interferometric measurement. However, the roll-pitch-yaw angles are not the exact definitions the metrologists expected in interferometry, because they require a certain sequential order of rotations and may cause errors in describing complicated rotations. The errors increase as the tip and tilt angles of the grating increase. Therefore, a replacement based on fused angles in robotics is proposed and named "fused-like angles." The fused-like angles are error-free, so they are more in line with the definitions in grating interferometry and more suitable for six-degree-of-freedom measurements. Fused-like angles have already been used in research on the kinematic model and decoupling algorithm of the six-degree-of-freedom grating interferometer.

1 Introduction

The grating interferometer has already stepped onto the six-degree-of-freedom (six-DOF) stage, using laser wavelength and grating pitch to measure translational and angular motions simultaneously. Besides high thermal inertia and low environmental sensitivity, six-DOF grating interferometers are usually smaller than laser interferometers because all the reading heads can be located on one side (Hu et al., 2019). Many different types of six-DOF grating interferometers have been proposed in the past years to fulfill the rigorous requirements of high-precision apparatus such as photolithography machines (de Jong et al., 2009; Li et al., 2014; Hsieh and Pan, 2015). More recently, research has gradually focused on the algorithms behind the optical structures of the reading heads. For example, Ye et al. published a couple of articles introducing error-free or ultraprecise algorithms for multi-DOF grating interferometers (Ye et al., 2018, 2019).

Orientations of the grating have usually been described in terms of roll-pitch-yaw angles (RPY angles). Being widely used in aviation and navigation, RPY angles are a certain type of Euler angle. With the help of rotation matrices, it is easy to calculate the rotation results on chips or by codes. However, different from the conventional RPY definition in avionics, the roll, pitch, and yaw angles for grating interferometers are custom-defined. For example, Cheng and Fan (2011) used yaw-roll-pitch to express rotations about the *x*, *y*, and *z* axes, while the order

used by Hsieh and Pan (2015) is yaw-pitch-roll. In other words, the definitions of RPY angles used in grating interferometry have a wider range than those in avionics. Thus, to be unambiguous, we use "custom-RPY angles" in this paper to describe those used in grating interferometry.

However, it is known that the matrix multiplications do not satisfy the commutative law. This means that when describing complicated rotations around multiple axes continually or simultaneously, custom-RPY angles are valid only with a pre-determined rotation order. Namely, different orders will lead to different orientations, although the corresponding values are the same. However, what we expect from a measurement system is a certain state of orientation, not a series of rotation angles. Thus, custom-RPY angles may cause inconvenience in building an accurate model of a six-DOF grating interferometer, and even errors when measuring the angular motions.

To overcome these disadvantages and meet the requirements of six-DOF grating interferometers, we began to give a novel definition for describing orientations instead of the roll, pitch, and yaw representation. We accidentally found that the fused angles, proposed by Allgeuer and Behnke (2015, 2018) for representing the orientation of a balancing body, are similar to the expected representations in six-DOF grating interferometry. Using the projections of the vectors for definitions and considering the actual requirements in six-DOF interferometers, we proposed "fused-like angles" to describe the orientation of the measured grating. This method can avoid the confusion caused by the custom-RPY angles and provide a clear and exact state of the orientation without the rotation order. The definition of the fused-like angles, the examples in describing orientations in six-DOF grating interferometers, and their advantages and applications are introduced and analyzed in the following sections.

2 Fused-like angles

2.1 Custom-RPY angles and their problems in describing the complicated rotations of grating interferometers

First, we define custom-RPY angles for description as was done in previous studies on grating

interferometers. As Fig. 1 shows, the main moving direction of a linear grating is defined as the x direction, which could be regarded as the front and rear. Rotation about the x axis is defined as the roll angle. Then the rotations about the y and z axes are defined as pitch and yaw angles, respectively. A six-DOF grating interferometer usually has a two-dimensional planer grating. To distinguish x and y directions, we still use linear gratings in Fig. 1 (and Fig. 6 below).
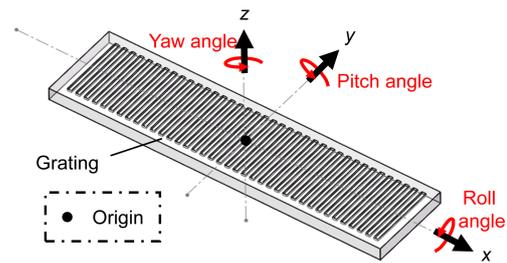

Fig. 1 Description of custom-RPY angles in this study
In grating interferometry, the normal vector of the grating is usually regarded as the z axis

On one hand, when expressing single-DOF rotations, results can be calculated by the corresponding rotation matrix in Eqs. (1)–(3):

$$R_x(\theta) = \begin{bmatrix} 1 & 0 & 0 \\ 0 & \cos\theta & -\sin\theta \\ 0 & \sin\theta & \cos\theta \end{bmatrix}, \quad (1)$$

$$R_y(\varphi) = \begin{bmatrix} \cos\varphi & 0 & \sin\varphi \\ 0 & 1 & 0 \\ -\sin\varphi & 0 & \cos\varphi \end{bmatrix}, \quad (2)$$

$$R_z(\psi) = \begin{bmatrix} \cos\psi & -\sin\psi & 0 \\ \sin\psi & \cos\psi & 0 \\ 0 & 0 & 1 \end{bmatrix}, \quad (3)$$

where θ, φ, and ψ represent the roll, pitch, and yaw angles, respectively. The custom-RPY angles are exact in handling cases with single-DOF rotations, for example, the tolerance analyses of grating interferometers (Cheng and Fan, 2011; Chang et al., 2019).

On the other hand, there is neither clear expression nor explanation of the complicated rotations in a grating interferometer, although researchers have already launched studies on six-DOF measuring systems. It is necessary to clarify whether custom-RPY is intrinsic or extrinsic.

It is easy to calculate the extrinsic rotation by left-multiplying these three matrices with a certain order:

$$R(\theta, \varphi, \psi) = R_z(\psi) R_y(\varphi) R_x(\theta). \tag{4}$$

Fig. 2 demonstrates the steps of the left multiplications in Eq. (4). The initial coordinate system is denoted by lowercase letters *x*, *y*, and *z*, two transition coordinate systems are denoted with prime marks, while the terminal one is denoted by capital letters *X*, *Y*, and *Z*.
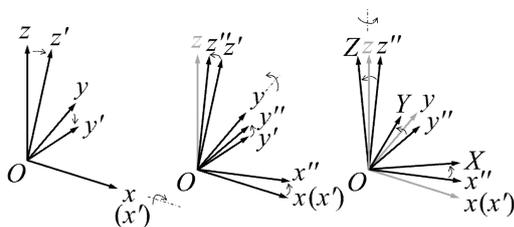

Fig. 2 Schematic of three rotation steps of extrinsic custom-RPY angles

However, in six-DOF grating interferometers, only the initial and terminal coordinate systems are physically defined. The transition ones are not entities in a real measuring system. Thus, it is difficult to determine the exact values of these angles with the coordinate systems *xyz* and *XYZ*.

As for the intrinsic rotations, the results can be calculated by matrices from Rodriguez's formula or with the help of the equivalence of extrinsic ones. Fig. 3 demonstrates the steps of the intrinsic custom-RPY angles. The denotations of coordinate systems are the same as those in Fig. 2.

The same problem, angles being defined with transition coordinate systems, exists in Fig. 3. The reason is that both the extrinsic and intrinsic rotations use matrix left-multiplication to calculate the attitude, so no matter what the order is, the latter angle is defined based on the previous rotation.

What we need to clarify is that we are not denying the effectiveness of the custom-RPY angles in describing active rotations, but using custom-RPY angles in six-DOF grating interferometry will cause some problems when representing passive orientations. For one thing, the rotation order should be pre-determined. A different order will lead to different rotation results, although the values are the same. For another thing, it may cause errors in tracing to the benchmarks.
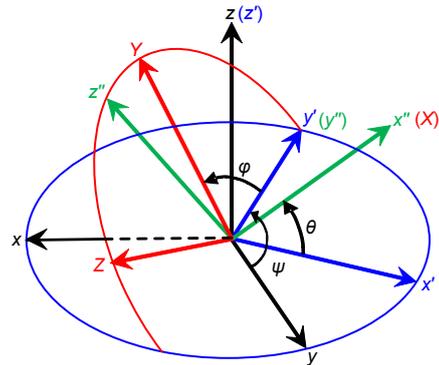

Fig. 3 Schematic of three rotation steps of intrinsic custom-RPY angles

As Fig. 4 shows, the benchmarks of a typical six-DOF grating interferometer are the laser wavelength and grating pitches. In ideal cases without mounting errors, the wavelength is always parallel to the *z* axis of the initial coordinate system (perpendicular to the ground), while the pitches of the planar grating are always parallel to the *X* and *Y* axes of the terminal coordinate system. Since the benchmarks are located in two different coordinate systems, the final six-DOF results of the grating should be transferred to the initial coordinate system.
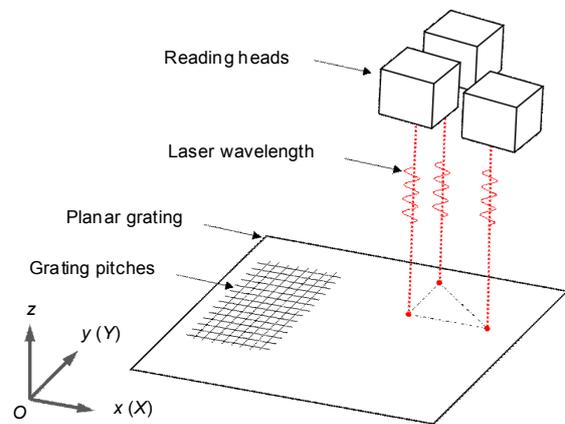

Fig. 4 Benchmarks of a typical six-DOF grating interferometer

Taking the laser wavelength in the initial coordinate system as an example, for a certain reading head, the Abbe principle tells us that the wavelength should be in line with the *z*-axis displacements. Similarly, to measure an angle with two differential displacements, the measured angle should be on a plane parallel to the differential displacements. Otherwise,

the inconsistency will cause an error (like the Abbe error).

From the analysis above, it is necessary to find another representation of the orientations. The expected representation should be a set of three independent angles without rotation orders and be consistent with the benchmarks.

2.2 Fused-like angles

The problems mentioned above also exist in robotics. In 2015, P. Allgeuer and S. Behnke first published an article about fused angles. It is helpful in working with rotations within major planes, not about the rotating axes, such as analyzing the balancing state of a body (Allgeuer and Behnke, 2015, 2018). The highlight of the fused angles is that the angles are defined with projections. Using the notations in Figs. 2 and 3, the fused roll and pitch are angles between the projections of the z axis and Z axis. It also has a tilt angle and a sign flag to distinguish the hemisphere.

Application in six-DOF grating interferometry is far away from that in robotics. The differences include that the ranges of the roll and pitch angles are quite small and the grating is impossible to turn over during measurement. Also, the Gimbal lock will not appear. So, considering the actual cases in interferometry and based on the projection definitions, we propose the "fused-like angles" to represent the orientation for six-DOF grating interferometers.

Ignoring the unused components, the fused-like angles have only three angles defined by two vectors: the normal vector of the grating and an auxiliary vector on the grating surface. As Fig. 5 shows, the normal vector is used to represent the fused-like roll and pitch, and the auxiliary vector is used to represent the fused-like yaw. Fig. 5 also illustrates that when

describing single rotations, the fused-like angles are the same as the other two representations. The vectors are all in the major planes of the initial coordinate system. Because only the upper hemisphere is considered, the ranges of fused-like roll and pitch are $(-\pi/2, \pi/2)$, while the fused-like yaw has a full range in $(-\pi, \pi]$. Such ranges are suitable for all type of gratings, including linear, planar, radial, and circular ones.
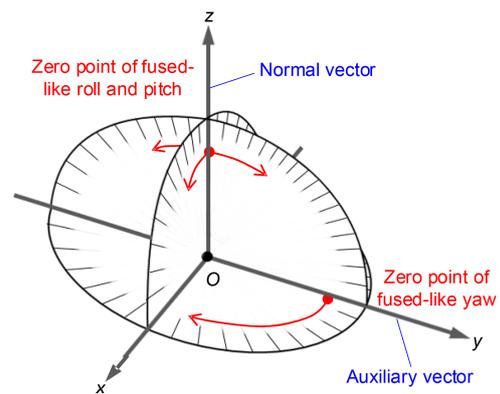

Fig. 5 Two vectors for defining the three fused-like angles
Zero points are determined by the vectors as well

Fig. 6 illustrates the cases with complicated rotations. As Fig. 6a shows, when the normal vector of the grating is out of the major planes, the fused-like roll and pitch can be defined as follows:

Roll: The fused-like roll θ is the angle between the z axis and vector $\boldsymbol{Z}_x$ (the projection of the Z axis on the yz plane).

Pitch: The fused-like pitch φ is the angle between the z axis and vector $\boldsymbol{Z}_y$ (the projection of the Z axis on the xz plane).

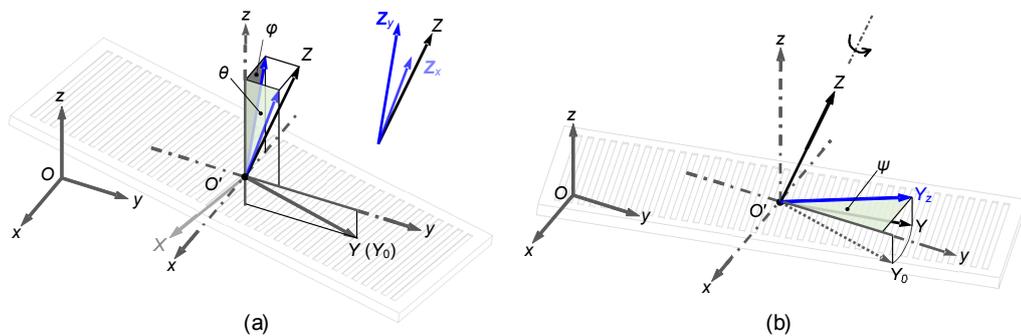The angles can be expressed by simple trigonometric formulae:

Fig. 6 Diagram of the fused-like angles: (a) roll and pitch; (b) yaw

$$\theta = \arctan(-Z_2 / Z_3), \qquad (5)$$

$$\varphi = \arctan(Z_1 / Z_3), \qquad (6)$$

where normal vector Z is represented as $Z=[Z_1\ Z_2\ Z_3]^\mathrm{T}$ in the initial coordinate system.

In the reverse direction, vector Z can be easily determined by fused-like roll and pitch:

$$Z \parallel \begin{bmatrix} -\tan\varphi & \tan\theta & 1 \end{bmatrix}^\mathrm{T}. \qquad (7)$$

A parallel symbol is used in Eq. (7) because such a form is simple and easy to understand but the vector is not normalized. When the grating rotates about the Z axis for a certain angle, as Fig. 6b shows, the fused-like yaw can be defined as follows:

Yaw: The fused-like yaw ψ is the angle between the y axis and the projection of auxiliary vector Y_z on the xy plane.

Similarly, supposing $Y=[Y_1\ Y_2\ Y_3]^\mathrm{T}$, the formulae of the yaw angle and auxiliary vector Y are expressed as

$$\psi = \begin{cases} \arctan(-Y_1 / Y_2), & Y_2 \geq 0,\ Y_1 \leq 0, \\ \pi - \arctan(Y_1 / Y_2), & Y_2 < 0, \\ 2\pi + \arctan(-Y_1 / Y_2), & Y_2 \geq 0,\ Y_1 > 0, \end{cases} \qquad (8)$$

$$Y \parallel \begin{bmatrix} -\sin\psi & \cos\psi & Y_k \end{bmatrix}^\mathrm{T}. \qquad (9)$$

Eq. (8) has a similar form to function atan2, but we still use basic trigonometric functions for clarity. Only the first and second items of vector Y are involved in the projection definition so that the third item Y_3 is undefined. It can be calculated from the fact that vectors Y and Z are perpendicular to each other:

$$Y_3 = \sin\psi \tan\varphi + \cos\psi \tan\theta. \qquad (10)$$

After locating vectors Y and Z, the other one, the X axis of the grating, can be easily calculated by cross product. Then, the orientation of the grating has been completely represented by Eqs. (5)–(10).

3 Conversion between the fused-like and custom-RPY angles

3.1 Relationship between fused-like and intrinsic custom-RPY angles

As we introduced above, fused-like and custom-RPY angles are two different representations of the same object; to simulate the angle differences of these two representations, it is important to analyze the conversion between them. This process is like using custom-RPY angles to find a certain orientation determined by the fused-like angles.

Comparing the rotation steps shown in Figs. 2 and 3, it is clear that the intrinsic rotation is the better choice because the extrinsic ones will lead to iterative calculation. Detailed rotations about three axes from the RPY angles to the fused-like angles are illustrated in Fig. 7. There are four parts: the left one is the initial state, while the following three show every step of the rotations. Axes of the initial coordinate system, results of the first and second rotations, and the target coordinate system are marked as xyz, $x'y'z'$, $x''y''z''$, and XYZ, respectively.
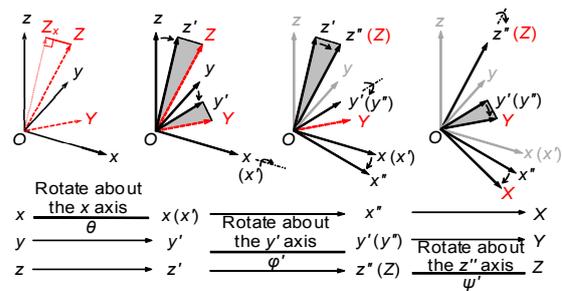

Fig. 7 Connecting the intrinsic custom-RPY angles and fused-like angles with three sequential rotations

In the initial state, the coordinate system is still in the starting orientation and the target coordinate system XYZ can be directly found by the fused-like angles. Then, after the first rotation about the x axis at roll angle θ, the coordinate system reaches the orientation denoted with one prime mark. The current normal vector of the grating, z', is parallel to the projection vector Z_x, which means that the fused-like roll and custom-RPY roll are the same. Actually, no matter what the rotation orders are, the first rotation will always be the same as that of the corresponding fused-like angles, because only one rotation matrix is left-multiplied. However, the difference occurs during the next rotation since the second matrix is also multiplied. The custom-RPY pitch is the angle about the y' axis between vectors z' and Z (highlighted by the shaded area), and this is different from the projection-involved definition above. To be unambiguous, a prime mark is added and the custom-RPY pitch can be expressed as

$$\varphi' = \text{sgn}\big((z' \times \boldsymbol{Z})_y\big)\arccos(z' \cdot \boldsymbol{Z}), \qquad (11)$$

where sgn() is the sign function, and subscript y means that the sign of the y (second) item determines the result. Likewise, the angle of the third rotation is different and the custom-RPY yaw is

$$\psi' = \text{sgn}\big((\boldsymbol{y}'' \times \boldsymbol{Y})_z\big)\arccos(\boldsymbol{y}'' \cdot \boldsymbol{Y}). \qquad (12)$$

With the help of Eqs. (11) and (12), the fused-like angles can be implemented by rotation matrices and the corresponding RPY angles. Numerical results can reflect the differences more clearly. The curves in Fig. 8 show the difference in pitch angles with different roll angles. Since the rotation angle at the wafer stage is only about several micro-radians, the unit of the vertical axis in Fig. 8 (and Fig. 9 below) is set as mrad. When the roll angles increase by one order of magnitude, the difference of magnitude between pitch angles will enlarge by two orders.
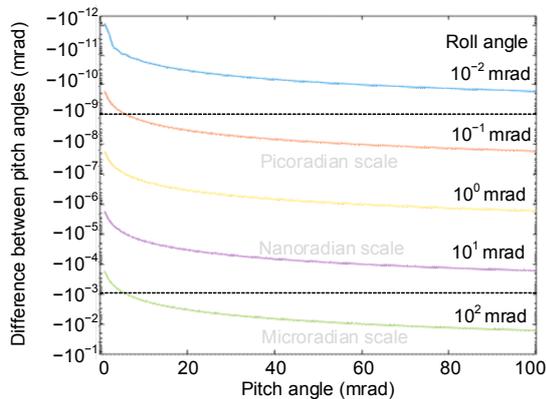

Fig. 8 Difference between the fused-like and RPY pitch angles (custom-RPY pitch−fused-like pitch) with different roll angles

Similar conclusions can be drawn from the curves in Fig. 9, showing the difference between the fused-like and RPY yaw angles. For each curve in Fig. 9, the roll and pitch angles are equal. Most of the data are negative but several near zero are positive, so the data are appropriately processed to fit the logarithm curves. The curves tell that the difference is related to the roll and pitch angles. Namely, the more the grating deviates from the initial state, the larger the differences will be.

Currently, the ranges of roll and pitch angles for a six-DOF grating interferometer for a photolithog-

raphy machine are about several mrad. It can be seen from Fig. 8 that the difference in pitch angles will be no larger than 1 nrad. Although this value is negligible, it will affect the six-DOF grating interferometry in two ways. For one thing, as the developing ranges of angles go higher, the difference will exceed the angular resolution and cause errors. For another thing, the existence of the difference is an obstacle in building the accurate kinematic model of the six-DOF grating interferometer.
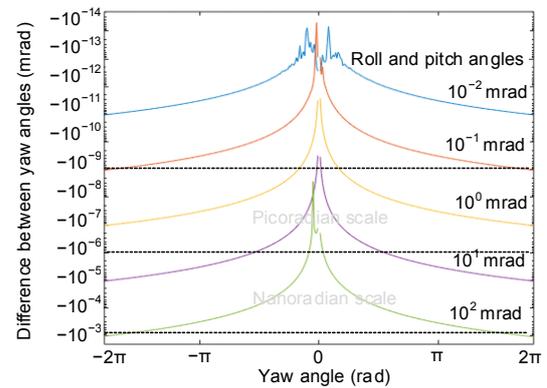

Fig. 9 Difference between the fused-like and RPY yaw angles (−|custom-RPY yaw−fused-like yaw|) with different roll and pitch angles
Roll and pitch angles are the same for each curve

3.2 Addable feature of fused-like angles

The fused-like angles are designed for grating interferometry, the incremental measurement method. The displacements measured by grating interferometers are the sum of phases at every instant. Thus, the addable fused-like representation is more suitable than the custom-RPY angles in the application for grating interferometers.

To describe the sum of the angles, the addition is used only in fused-like representations:

$$\boldsymbol{Z} \parallel \big[-\tan(\varphi_0 + \varphi_1) \quad \tan(\theta_0 + \theta_1) \quad 1\big]^{\text{T}}, \qquad (13)$$

$$\boldsymbol{Y} \parallel \big[-\sin(\psi_0 + \psi_1) \quad \cos(\psi_0 + \psi_1) \quad Y_3\big]^{\text{T}}, \qquad (14)$$

where the subscripts are used to distinguish these two addends. When using custom-RPY angles, the calculation is very complicated:

$$\boldsymbol{Z} = R(\theta_1, \varphi_1, \psi_1)\big[R(\theta_0, \varphi_0, \psi_0)z\big]. \qquad (15)$$

However, complexity is not the most severe problem. As discussed above, the rotation axes of RPY angles are not fixed, so even for the same angle, there is not a fixed standard for addition. To put it simply, θ_0 plus θ_1 is not equal to $\theta_0+\theta_1$ in the custom-RPY angles.

Fig. 10 offers a graphic explanation. Suppose that the grating has sequential rotations implemented by rotation matrices, and the roll, pitch, and yaw angles are all set as 1 mrad in every step. The orientation of the grating is represented by the fused-like angles. The expected angles are shown as the black dashed line, but all the solid curves for actual results have deviations. In addition, these solid curves are not straight—the deviations become higher as the cumulative angles increase. It shows that custom-RPY angles with changing rotation axes may not be suitable for the six-DOF grating interferometer, but the fused-like angles could overcome this disadvantage.
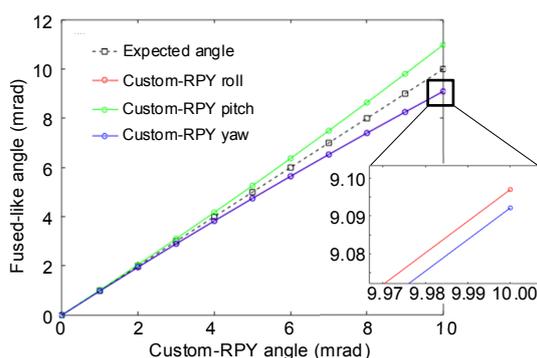

Fig. 10 Sequential custom-RPY rotations by rotation matrices and their representation by the fused-like angles

4 Conclusions

In this paper, we proposed a representation method for describing the orientations in a six-DOF grating interferometer as the replacement for the currently used custom-RPY angles. The method is composed of three angles whose definitions involve projections of vectors. This idea comes from the fused angles in robotics; thus, we name the proposed method "fused-like." With the fused-like angles, the orientation of the measured grating can easily be described by basic trigonometric functions.

Note that we are not criticizing the Euler angles and the rotation matrices but just introducing a better representation for application to six-DOF grating

interferometry. Different features make the two representations suitable for different uses. The fused-like angles have no rotation order and the addition and subtraction of the fused-like angles are commutative. These factors make it helpful in describing the orientation of the grating in six-DOF interferometry. The RPY angles are calculated by rotation matrices with a certain order, so they have better performance in handling sequential single-axis rotations, such as the articulated arm coordinate measuring machine (AACMM). A brief comparison is listed below.

The fused-like angles are based on a fixed coordinate system, while the RPY angles are based on changing rotation axes. The fused-like angles can be defined by single trigonometric functions but the RPY angles are calculated by rotation matrices. Thus, the fused-like angles are addable and independent of each other; the calculation of RPY angles is not commutative or coupled.

The fused-like angles can make an accurate representation of the measured grating, only with the round-off error in the computer. They have already been used in building the kinematic model and deriving the error-free decoupling algorithm of the six-DOF grating interferometer. We believe that the proposed fused-like angles have potential in similar six-DOF measuring instruments such as laser interferometers or capacity transducers, but the specific definitions might be slightly different because of the difference in locations of their benchmarks.

References

Allgeuer P, Behnke S, 2015. Fused angles: a representation of body orientation for balance. IEEE/RSJ Int Conf on Intelligent Robots and Systems, p.366-373.
https://doi.org/10.1109/IROS.2015.7353399
Allgeuer P, Behnke S, 2018. Fused angles and the deficiencies of Euler angles. IEEE/RSJ Int Conf on Intelligent Robots and Systems, p.5109-5116.
https://doi.org/10.1109/IROS.2018.8593384

Chang D, Xing X, Hu PC, et al., 2019. Double-diffracted spatially separated heterodyne grating interferometer and analysis on its alignment tolerance. *Appl Sci*, 9(2):263. https://doi.org/10.3390/app9020263

Cheng F, Fan KC, 2011. Linear diffraction grating interferometer with high alignment tolerance and high accuracy. *Appl Opt*, 50(22):4550-4556. https://doi.org/10.1364/AO.50.004550

de Jong F, van der Pasch B, Castenmiller T, et al., 2009. Enabling the lithography roadmap: an immersion tool based on a novel stage positioning system. Proc Optical Microlithography XXII, 7274:72741S. https://doi.org/10.1117/12.814254

Hsieh HL, Pan SW, 2015. Development of a grating-based interferometer for six-degree-of-freedom displacement and angle measurements. *Opt Expr*, 23(3):2451-2465. https://doi.org/10.1364/OE.23.002451

Hu PC, Chang D, Tan JB, et al., 2019. Displacement measuring grating interferometer: a review. *Front Inform Technol Electron Eng*, 20(5):631-654. https://doi.org/10.1631/FITEE.1800708

Li XH, Shimizu Y, Ito T, et al., 2014. Measurement of six-degree-of-freedom planar motions by using a multi-probe surface encoder. *Opt Eng*, 53(12):122405. https://doi.org/10.1117/1.OE.53.12.122405

Ye WN, Zhang M, Zhu Y, et al., 2018. Translational displacement computational algorithm of the grating interferometer without geometric error for the wafer stage in a photolithography scanner. *Opt Expr*, 26(26):34734-34752. https://doi.org/10.1364/OE.26.034734

Ye WN, Zhang M, Zhu Y, et al., 2019. Ultraprecision real-time displacements calculation algorithm for the grating interferometer system. *Sensors*, 19(10):2409. https://doi.org/10.3390/s19102409